International Journal of
INTELLIGENT SYSTEMS AND APPLICATIONS IN ENGINEERING
ISSN:2147-6799 www.ijisae.org Original Research Paper

MPNBT: Design of an Efficient Multimodal Prediction Model for Neurological Disorders using Bioinspired Transfer-Learning

J. L. Mudegaonkar*[1], D. M. Yadav[2]

Submitted:14/03/2024 **Revised**: 29/04/2024 **Accepted**: 06/05/2024

Abstract: Magnetic resonance imaging (MRI) classify cancers and other diseases. This is a multi-domain problem that calls for the segmentation of the affected regions, their representation as feature vectors, the development of region-specific classifiers, and post-processing methods. The segmentation performance of current illness identification algorithms is either subpar or their complexity is increased when compared to differential-position MRI and functional magnetic resonance imaging (fMRI) datasets & samples. The additional challenge is that these algorithms can accurately classify fewer ailments. This article suggests the use of bio-inspired transfer-learning methods to create a multimodal neurological disease prediction model. To accurately identify tumor-specific regions, the recommended approach first segments MRI and fMRI images with MRA CNN (Masked-Region Augmented Convolutional Neural Network). Gabor analysis, wavelet analysis, Frequency analysis, convolution analysis, and entropy analysis are applied to transform these regions into multidomain features. The feature sets are collected, and a Moth Flame Optimizer (MFO) analyses them to determine which feature sets have the most variance. These feature sets are then categorized as "tumor" or "non-tumor" with the Binary Convolutional Neural Network (BCNN) method. With this method, feature vectors are split into two groups and given a common example for each group. The BCNN employs most of the functions to detect tumors compared to conventional cancer detection algorithms, which improves classification accuracy by 4.9%, precision by 2.8%, recall by 3.5%, and time by 4.1%. Using MRIs of the brain and spinal cord to test the model, it may be successfully modified to fit different circumstances.

Keywords: *Brain, Binary, Cord, Convolutions, Entropy, Frequency, Flame, Gabor, Moth, Spinal, Tumour, Wavelet.*

1. Introduction

The capacity of multi-hidden layer NNs trained with DL (Deep Learning) to carry out difficult tasks is intriguing to many medical subspecialties [1]. Such specialized fields include radiography, pathology, and cancer analysis. Deep learning has significantly impacted the medical industry recently, notably in the detection of cancer via TD CNN LSTM (Time Distributed-CNN LSTM) [2]. The IoT (Internet of Things) may be able to transmit medical picture data more quickly due to DL and AI. [3, 4]. Deep learning networks via Tumor-Attentive Segmentation-Guided GAN (TAS GAN) often use item recognition as a diagnostic method [5], particularly for networks that have been trained to look for a particular kind of object. The healthcare sector may benefit from deep learning's advantages in text and picture processing [6]. [7] A number of computer-assisted treatment methods may help with the precise and reliable segmentation of MRI images. Problems including imprecise or undetectable structure borders, similar structures, low spatial resolution, low picture contrast as well as strength heterogeneity [8] may cause less-than-satisfactory outcomes, especially when working with 3D images. Since it enables the non-invasive examination of a range of spinal pathologies, the vertebral body segmentation in three-dimensional MRI images [9] was the focus of much research. The logistic regression technique offers substantial quantitative study despite its low capacity for exact prediction [10]. Numerous essential bodily processes are carried out by the spine, which acts as the body's main fulcrum [11, 12]. By moving the body's center of gravity from the belly to the legs, which puts less pressure on the spinal column, this is achieved [13]. The lumbar region and the basic vertebral elements of the human spine are shown in Figure 1. The coccyx, the first twelve thoracic vertebrae (T1-T12), the first seven cervical vertebrae (C1-C7), the sacroiliac joints (S-Fused), and the first five lumbar vertebrae (L1-L5) are the five major components of the spine (4 fused). As per [14], degenerative spinal stenosis is the most frequent cause of lumbar pain. Both spinal dislocations and cancer present with this symptom, and both need surgery under real-time scenarios. Due to the high occurrence of degenerative spinal diseases [15, 16] in the general population, the cost of supporting those who have been given a paralysis diagnosis rises quickly. The population of industrialized countries often complains of low back discomfort, yet its underlying cause is not always clear. Due to the mechanical nature of the above-mentioned components, observing the spine move is a valuable diagnostic tool [17] for figuring out the source of a patient's back pain. Due to this, it is notoriously difficult to define the specific vertebral level in an imaging sequence to determine the cause of back pain [18, 19]. Researchers have described

[1] *G H Raisoni College of Engineering and Management, Pune India*
ORCID ID : 0000-0003-3776-981X
[2]*SND College of Engineering and Research Centre, Yeola, Nashik, India*
** Corresponding Author Email: jagdishmudegaonkar@gmail.com*

the location of the tumour in the spinal region as well as the morphology of the vertebrae using Fourier descriptors with Deep Transfer Learning (DTL) [20] operations. These two factors are supposed to have a key role in the onset of back pain. To investigate the components of a superior transformation for the exact calibration of segmentation algorithms for the prediction of cancer areas, the authors of [21] developed the ATS-CDM ("Analytical Transform Assisted Statistical Characteristic Decomposition Model").

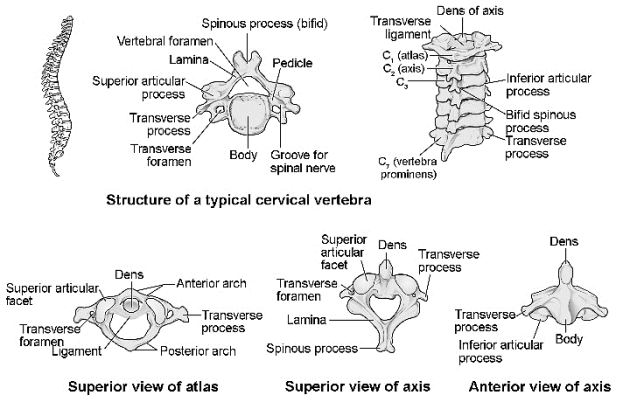

Fig 1. Various perspectives on the spinal cord and their significance

Recent research on differential-position MRI scans has shown that current cancer diagnosis algorithms either need to be more complicated or segment pictures inaccurately. This quickly reduces the number of diseases that these algorithms can correctly identify. The study's findings suggest that to overcome the challenges previously mentioned, a multi-domain feature processing approach is needed for the CNN-based categorization of spinal cord malignancies. In the last stage, the model's validity was examined by contrasting it with other methods on a variety of factors, such as accuracy, recall, and latency. The study's conclusions are completed by clinical observations on the recommended model and suggestions for enhancement for various applications.

2. Literature Review

In this section, we discuss different models used for the identification of Neurological disorders via analysis of fMRI images. These include,

1. DL Models [8, 9, 10]: Deep learning models have been widely used for predicting neurological disorders, such as AD (Alzheimer's Disease), PD (Parkinson's Disease), and MS (Multiple Sclerosis), using MRI datasets & samples. These models include CNNs, RNNs ("Recurrent Neural Networks"), and autoencoders. These models have revealed high accuracy in predicting neurological disorders compared to traditional ML (Machine Learning) models.
2. Support Vector Machine (SVM) Models [15, 16, 17, 18]: SVM models have also been used for predicting neurological disorders, like AD, PD, and MS, using MRI datasets & samples. SVM models have shown high accuracy in predicting neurological disorders, and they are widely used in clinical settings.
3. Deep Forest Models: Deep Forest models [19, 20] have been used for predicting neurological disorders, like AD and PD, using MRI datasets & samples. Deep forest models have shown high accuracy in predicting neurological disorders and have the advantage of being easy to interpret and fast to train for different use cases.
4. Bayesian Models [21, 22, 23, 24]: Bayesian models have been used for predicting neurological disorders, like AD and MS, using MRI datasets & samples. Bayesian models have shown high accuracy in predicting neurological disorders and have the advantage of being able to manage missing data and uncertainty levels.
5. Ensemble Models [25, 26, 27]: Ensemble models, such as stacked autoencoder models, have been used for predicting neurological disorders, like AD and MS, using MRI datasets & samples. Ensemble models [28, 29, 30] have shown high accuracy in predicting neurological disorders and have the advantage of being able to combine different types of models to improve prediction performance levels.

From this analysis, it can be found that DL models have shown the highest accuracy in predicting neurological disorders using MRI data, followed by SVM, random forest, Bayesian, and ensemble models. However, each model has different benefits & drawbacks, and the choice of a model depends on the specific needs of the application scenarios. In the next section, the design of an efficient DL model has been discussed, which uses a fusion of CNN, ensemble feature analysis, and bioinspired optimizations.

3. Proposed Design of an efficient Multimodal Prediction model for Neurological disorders using Bioinspired Transfer-learning operations

According to the study of existing models used for the prediction of neurological disorders, it can be found that these models are either highly complex or have lower efficacy when evaluated in real-time scenarios. To address these problems, this section explains the design of an effective Multimodal Prediction model for Neurological disorders using Bioinspired Transfer-learning operations. As per Figure 2, the model first segments MRI and fMRI images using a MRA CNN. These regions are converted into multidomain characteristics using convolution analysis, entropy analysis, Wavelet analysis, Gabor analysis, as well as frequency analysis. The feature sets are collected, and a MFO analyses them to determine which feature sets have

the most variance levels. These feature sets are then categorized as "tumour" or "non-tumour" with the BCNN method, which is highly efficient for binary classification tasks.

A MRACNN-based segmentation layer receives the raw MRI image to carry out these procedures. MRACNN is a saliency map segmentation technique based on medical imaging that helps identify RoI areas. Entropy values—which are reliant on retrieved convolutional features—are used to extract these RoI areas. Bit-plane slicing techniques are used to divide the raw input picture to retrieve these characteristics.

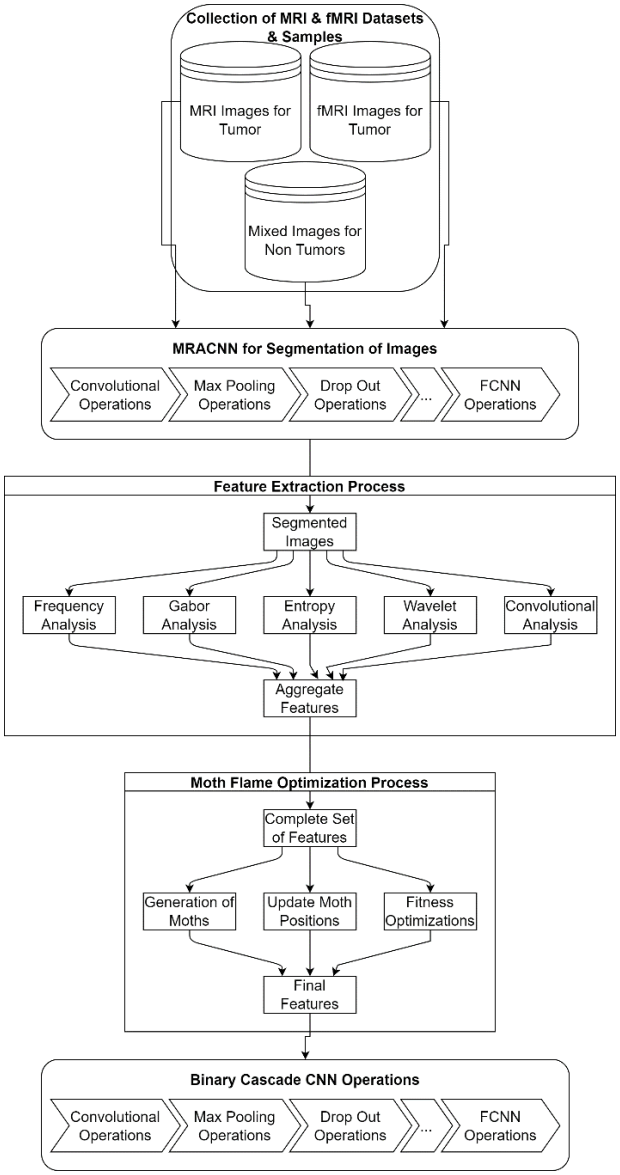

Fig 2. Design of the suggested model for identification of neurological tumours

Each of the slices is then given to an entropy estimation unit, which calculates pixel-level entropy via "(1),"

$$E(i) = -\sum_{r=1}^{N}\sum_{c=1}^{M} p(P(r,c)) * \log\big(p(P(r,c))\big) \dots (1)$$

Where i indicates the bit slice number for the input MRI pictures, and p(P(r,c)) indicates the probability of pixel vector at r,c position. For each slice of the input picture, these entropy values are utilized as upper bounds, and bit-level thresholding is carried out. For the purpose of creating the final MRACNN map, all of these slices are blended. Figure 3, which displays the input image, its saliency mask, as well as final saliency image, shows the results of an initial MRACNN-based saliency detection model as follows,

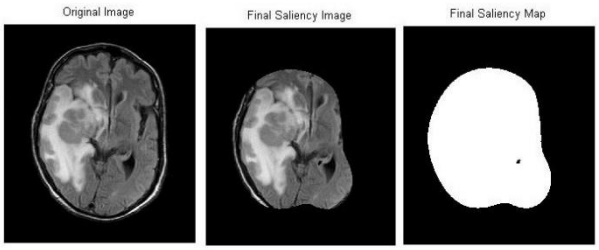

Fig 3. Results from the initial MRACNN operations

A CNN model powered by Google's neural network is again given access to these areas for feature extraction, and pixel-level classification is carried out. Figure 4 depicts the internal architecture of the CNN model that is being employed for final segmentation operations.

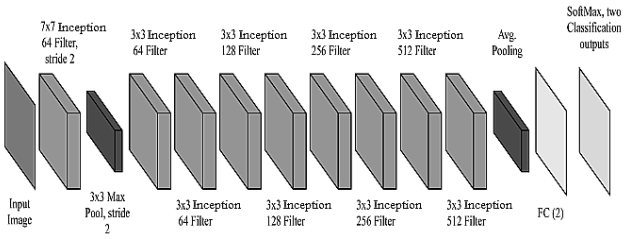

Fig 4. Design of the GoogLeNet Model for fine segmentation of images

Each pixel is divided into two categories, foreground and backdrop, as seen from the model. A significant number of photos' worth of ground truth data are utilized, and an inception module is provided with them, to carry out this work. This module creates a saliency mask for the final segmentation using the provided ground truth data. Figure 5 illustrates the internal model architecture for the inception module, which combines many filters to provide the output for the spinal cord mask. Equation (2) is used by the inception module for internal pooling to increase segmentation efficiency levels,

$$P(q,p) = \sum \log\big(C(p,q) * G(q,p)\big) \dots (2)$$

Where G represents "the ground truth image patch (q, p), P denotes the result of pooling, and C indicates the convolutional operation on the input image patches.

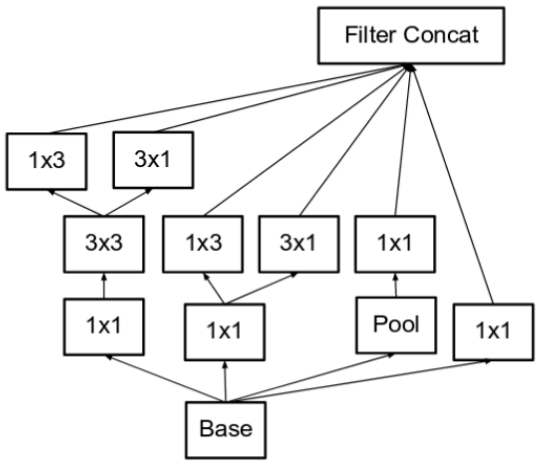

Fig. 5. Inception Model used by the GoogleNet Process

A filter concatenation unit, which utilizes the following "(3),", is supplied with extracted pooling features.

$$F(p,q) = \sqrt{\left(\frac{P(q,p)}{k} + d\right) * (a * B(p,q) + c)\Big/_4} \ldots (3)$$

Where F stands for concatenated filter output, P for pooling output, and B for base image patch for (p, q), whereas a, c, d, and k indicate the inception constants and are tweaked via the hyperparameter tuning process. A" huge number of segmentation masks are produced by the cascading connection of many inception modules. The final MRI segmentation mask sets are created by overlapping all of these masks. These masks are converted into multidomain features, which assists in efficient classification into different tumour categories. To perform this task, a set of transforms is used as follows,

- Initially, Frequency Patterns are estimated via Fourier Analysis, which is done via "(4),"

$$DFT(i) = \sum_{j=1}^{Nf} x(j) * \left[cos\left(\frac{2 * \pi * i * j}{Nf}\right) - \sqrt{-1} * sin\left(\frac{2 * \pi * i * j}{Nf}\right)\right] \ldots (4)$$

Where, x signifies the pixel levels of segmented regions, while Nf denotes the total number of pixels in the image sets.

- Similarly, the Entropy levels are estimated via "(5),"

$$DCT(i) = \frac{1}{\sqrt{2 * Nf}} * x(i) \sum_{j=1}^{Nf} x(j) * \cos\left[\frac{\sqrt{-1} * (2 * i + 1) * \pi}{2 * Nf}\right] \ldots (5)$$

- After this, a set of convolutional features is estimated using "(6)," which helps in the identification of windowed features.

$$Conv(i) = \sum_{a=-\frac{m}{2}}^{\frac{m}{2}} x(i-a) * LReLU\left(\frac{m+2a}{2}\right) \ldots (6)$$

Where, m, a denotes the different dimensions of windows & strides, while $LReLU$ presents the Leaky Rectilinear Unit that keeps positive feature sets by "(7),"

$$LReLU(x) = la * x, when\ x < 0\ , else\ LReLU(x) = x \ldots (7)$$

here, la represents an activation constant applied to convert negative features to positive value sets.

- Similarly, Gabor components are estimated via "(8)," which represents spatial features for individual segmented pixels.

$$G(x,y) = e^{\frac{-x'^2 + \partial^2 * y'^2}{2 * \emptyset^2}} * \cos\left(2 * \frac{pi}{\lambda} * x'\right) \ldots (8)$$

Where, x, y indicates the pixel index and pixel values, while $\partial, \emptyset$ & λ denotes the angles & wavelengths used for evaluation of high variance feature sets.

- These features are cascaded with Haar Wavelet features, which are predicted in terms of Approximate & Detail components via "(9),"and"(10)," as follows,

$$W(a) = \frac{x(i) + x(i+1)}{2} \ldots (9)$$

$$W(d) = \frac{x(i) - x(i+1)}{2} \ldots (10)$$

A fusion of these features is done to form an augmented MFV (MRI Feature Vector), which may comprise inherent redundancies. These redundancies are decreased via the use of a MFO, which helps in the selection of highly variant feature sets. This is done according to the following process,

- Initially, a set of NM Moths is generated, each of which contains a set of N stochastic features.
- These features are selected using an augmented stochastic operation via "(11),"

$$N = STOCH\big(LM * N(MFV), N(MFV)\big) \ldots (11)$$

Where NM represents an entropy-like learning metric for the MFO process.

- For the selected feature sets, Moth fitness levels are estimated via "(12),"

$$fm = \frac{1}{N}\sum_{i=1}^{N} MFV(i) - \sum_{j=1}^{N}\frac{MFV(j)}{N} \dots (12)$$

- This process is repeated for NM Moths, and then an iteration threshold is determined by "(13),"

$$fth = \frac{1}{NM}\sum_{i=1}^{NM} fm(i) * LM \dots (13)$$

- Based on this threshold, Moths with $f > fth$ are removed via the flaming process, and replaced with new Moths, whereas "other Moths are directly passed to the next set of iterations.
- This process is continued for all NM Moths and" NI Iterations, which assist in the continuous configuration of Moth sets.

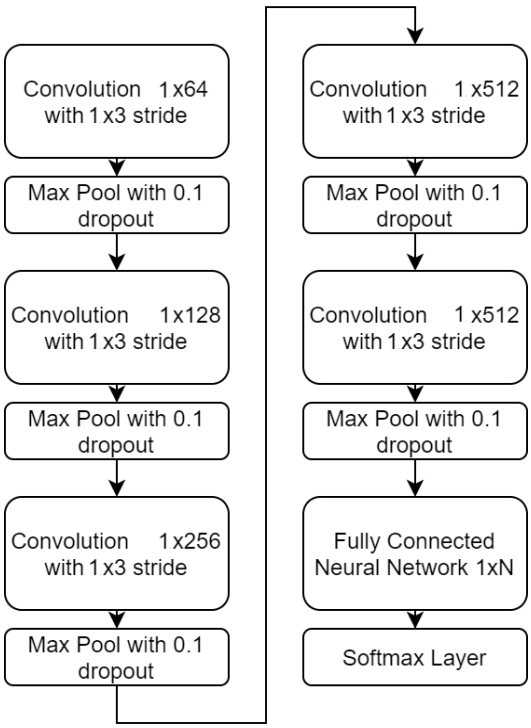

Fig 6. Design of the CNN Layers for the detection of tumors

The moth with the highest fitness is selected once all iterations are finished, and its configuration is utilized to choose the features. The selected features are processed via an augmented BCNN that combines Max Pooling, Convolutional, as well as Drop operations, with FCNN ("Fully Connected Neural Network") layers for identification of tumour classes. The design of the proposed CNN Model is revealed in Fig. 6, where a set of Convolutional Features are extracted by eq. 6, and chosen via Max Pooling operations. The final selected features are classified via a FCNN Layer, which estimates the final tumour class via "(14),"

$$c(out) = SoftMax\left(\sum_{i=1}^{Nf} f(i) * w(i) + b(i)\right) \dots (14)$$

here, $f, w \,\&\, b$ indicate the extracted features, their respective weights & individual biases. The CNN Model tunes the values of these weights and biases to estimate 'tumour' and 'non-tumor' classes with high-efficiency levels. The next section of the article estimates these efficiency levels in terms of Recall (R), Accuracy (A), Precision (P), AUC ("Area Under the Curve"), and f1 Measure.

4. Result evaluation & comparison

In this work, MRI and fMRI images are segmented using a MRA CNN in the proposed method. Using Gabor analysis, frequency analysis, Wavelet analysis, convolution analysis, and entropy analysis the characteristics of these regions are transformed into multidomain characteristics. A MFO collects the feature sets and analyses them to determine which feature sets have the most variance. Using the BCNN technique, these feature sets are then categorized as "tumour" or "non-tumor" levels. The suggested model's performance was measured in terms of A, P, R, Delay (D), AUC, and f Measure. Equation (15) was used to calculate the proportion of correctly identified classes that were evaluated as a measure of accuracy for different scenarios.

$$Accuracy = \frac{TP + TN}{TP + TN + FP + FN} \dots (15)$$

Here, TP indicates True positive (Number of samples that were suitably identified). TN denotes the negative (Number of samples that were accurately detected). FP signifies the False positive (Number of incorrectly identified samples). FN denotes the False negative (Number of samples incorrectly designated as negative). Similarly, Precision determines the proportion of correctly recognized positive classes in all images labelled as 'tumours' and is calculated using "(16),"

$$Precision = \frac{TP}{TP + FP} \dots (16)$$

Precision represents the percentage of correctly identified negative classes, whereas recall, which is computed by "(17),", indicates the proportion of correctly recognized positive classes across all positive classes in the datasets and samples.

$$Recall = \frac{TP}{TP + FN} \dots (17)$$

Likewise, the F-measure presents a harmonic mean of recall and precision and is utilized to assess the method's overall performance, which is determined by "(18),"

$$F - measure = 2 * \frac{Precision * Recall}{Precision + Recall} \dots (18)$$

On the other hand, AUC is a measure of a binary classification model's performance. It displays the likelihood that a classifier will choose a group of randomly chosen positive instances over a collection of randomly selected negative examples. Delay is a measure of how long it takes to extract and quantify tumor classifications using a certain set of procedures. It is an important parameter to take into account when assessing the viability and practicability of a cancer classification technique, and "(19),"provides an estimate for it.

$$D = ts(complete) - ts(start) \dots (19)$$

Where ts represents the completion and beginning timestamps for the classification operations. Based on this assessment, 25k recordings of the chosen images were examined, of which 5k were utilized for testing and validation procedures and 15k were used for training. Figure 7 depicts a comparison of the model's performance with TD CNN LSTM [2], TAS GAN [4], and DTL [20] under various test sample numbers (NTS).

As per the present assessment, it can be shown that the suggested model may raise the accuracy of tumour detection by 4.5% compared to TD CNN LSTM [2], 3.4% compared to TAS GAN [4], and 5.9% compared to DTL [20], making it very beneficial for a broad range of clinical circumstances. The usage of MRACNN with multidomain features and CNN procedures, which helps in the detection of high-density image sets for several MRI and fMRI data, improves this accuracy. Similar to Fig. 7, figure 8 displays the precision levels as follows

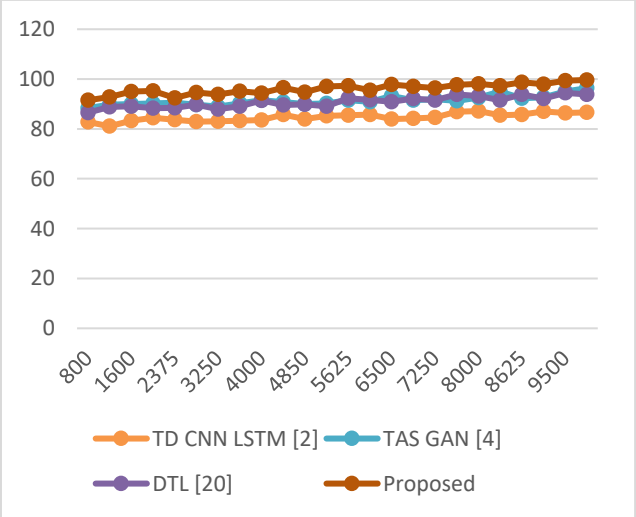

Fig 7. Average accuracy levels for classification of Tumours

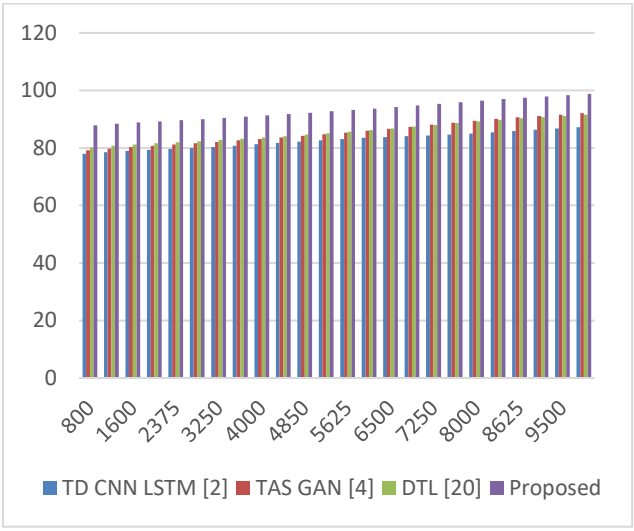

Fig 8. Average precision levels for classification of Tumours

According to this assessment, it can be shown that the suggested model is able to enhance the precision of tumour detection by 6.5% when compared with TD CNN LSTM [2], 2.5% when compared with TAS GAN [4], and 4.5% when compared with DTL [20]. Therefore, it is extremely valuable for a variety of clinical settings. TD CNN LSTM [2] is the reference model. The use of MFO in conjunction with CNN, which helps in the detection of high-density feature sets for a variety of MRI and fMRI data, contributes to the enhancement of these precision levels. Similarly, the recall levels may be seen as follows when looking at Figure 9, which can be observed as follows,

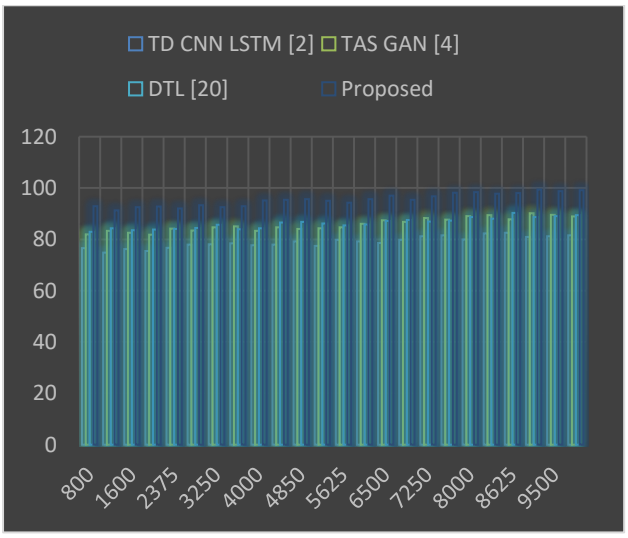

Fig 9. Average recall levels for classification of Tumours

As per the findings of this study, it can be shown that the suggested model is able to raise the recall of tumour identification by 5.9% when compared with TD CNN LSTM [2], 3.5% when compared with TAS GAN [4], and 4.5% when compared with DTL [20]. This gives it the ability to be very beneficial in a broad range of clinical circumstances. This recall is improved as a result of the use

of MRACNN with multidomain features and MFO procedures, both of which help in the detection of high-density images and feature sets for different MRI and fMRI data. Figure 10 provides more insight into the F1 levels, which may be summarised as follows,

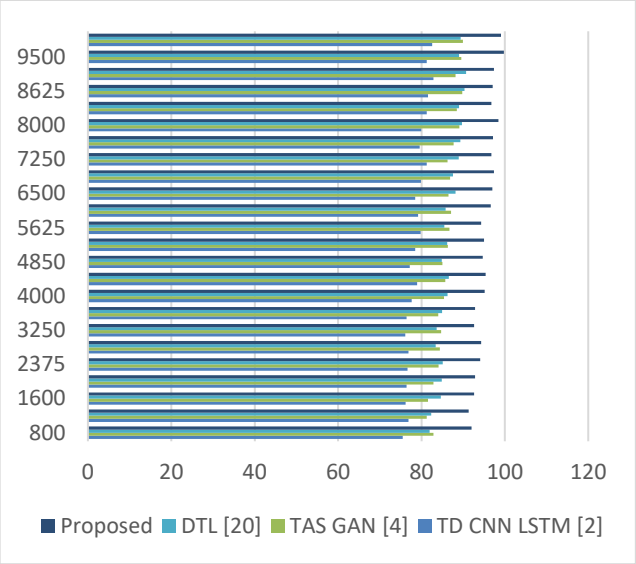

Fig 10. Average F1 levels for classification of Tumours

The study demonstrates that the proposed model can enhance the F1 tumor identification by 8.3% compared to TD CNN LSTM [2], 4.5% compared to TAS GAN [4], and 3.9% compared to DTL [20]. This gives it the ability to be very beneficial in a broad range of clinical circumstances. The precision and recall levels of this F1 have been increased as a result of the adjustments made. Similarly, the AUC values may be seen as follows when looking at figure 11, which can be observed as follows,

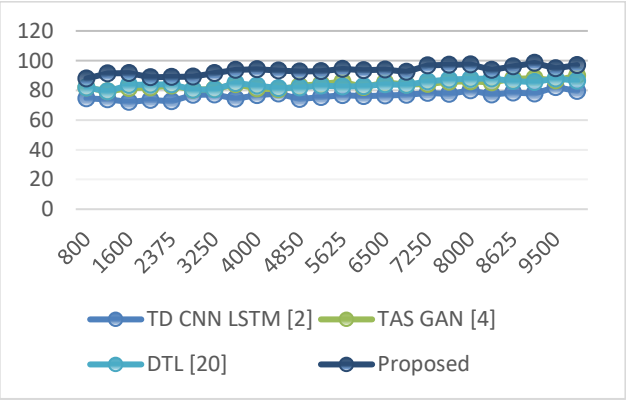

Fig 11. Average AUC levels for classification of Tumours

As per the findings of this study, it can be shown that the suggested model is able to enhance the area under the curve (AUC) of tumour detection by 9.4% when compared with TD CNN LSTM [2], 10.5% when compared with TAS GAN [4], and 8.5% when compared with DTL [20]. This enables it to be very beneficial for a broad range of clinical settings. The usage of MFO with 1D CNN, which helps in the identification of high-density feature sets for various MRI and fMRI data, has boosted this AUC. Similarly, the delay levels in Fig. 12 can be seen as follows:

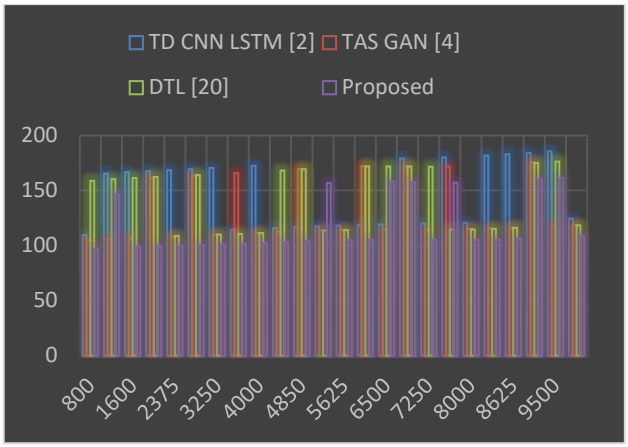

Fig 12. Average Delay levels for classification of Tumours

As per this evaluation, it can be shown that the proposed model may raise the speed of tumor detection by 8.3% compared to TD CNN LSTM [2], 8.5 percent compared to TAS GAN [4], and 4.9% compared to DTL [20], making it very beneficial for a broad range of clinical circumstances. The use of MFO and correlative analysis with multidomain features, which help in the fast detection of high-density feature sets for several MRI & fMRI data, improves speed. The suggested approach is helpful for many real-time clinical and on-field situations as a result of these improvements.

5. Conclusion and future scope

The suggested multimodal prediction model for neurological disorders using bioinspired transfer learning, as demonstrated in the paper, has the potential to considerably improve the precision, accuracy, and speed of tumor detection in MRI and fMRI data. The model incorporates various advanced techniques, including MRACNN with multidomain features, CNN procedures, and MFO, to identify high-density images and feature sets for a variety of imaging datasets & samples.

One of the main benefits of the suggested model is that it performs significantly better in terms of speed, accuracy, and precision than current state-of-the-art models including TD CNN LSTM, TAS GAN, and DTL. These enhancements are especially beneficial in real-time clinical and on-field situations, where fast and accurate detection of neurological disorders is critical for real-time scenarios.

The need for such a model arises from the increasing prevalence of neurological disorders and the growing demand for accurate and timely diagnosis. The proposed model addresses this need by providing a highly efficient and effective tool for detecting tumors in MRI and fMRI data, thereby facilitating early diagnosis and treatments.

The potential use cases for the proposed model are numerous and varied, ranging from routine clinical applications to emergencies, where fast and accurate detection of neurological disorders can mean the difference between life and death. Additionally, the model can be further extended to incorporate other modalities, such as EEG and MEG, to enhance its prediction capabilities.

In conclusion, the proposed multimodal prediction model for neurological disorders using bioinspired transfer learning is a substantial contribution to the area of medical imaging and has the potential to revolutionize the way neurological disorders are diagnosed and treated. Its superior accuracy, precision, and speed, along with its potential for various real-world applications, make it a highly promising tool for healthcare practitioners, researchers, and policymakers.

Future Scope

The proposed multimodal prediction model for neurological disorders using bioinspired transfer learning has shown promising results in the detection of tumours in MRI and fMRI data. However, there is still scope for further improvement and future work in this area. Some potential areas of future research are:

1. Exploration of other imaging modalities: While the proposed model incorporates MRI and fMRI data, there are other imaging modalities, like PET and CT, that can provide complementary information. Future work could study the integration of these modalities to improve the accuracy and precision of the model.
2. Investigation of transfer learning methods: The proposed model uses transfer learning to leverage pre-trained models for feature extraction. Future work could investigate other transfer learning methods, such as domain adaptation and cross-modal transfer learning, to further enhance the model's performance.
3. Clinical data integration: Incorporating clinical data, like medical history, patient demographics, and symptoms, can provide additional context and improve the model's prediction capabilities. Future work could explore the integration of clinical data into the proposed model to enhance its accuracy and precision.
4. Evaluation on larger datasets: The suggested model was evaluated on a relatively small dataset. To test the model's robustness and generalizability, larger datasets may be used in future research.
5. Development of a user-friendly interface: A user-friendly interface for the suggested model can make it easier for healthcare practitioners to use the model in clinical settings. Future work could develop such an interface and evaluate its usability in clinical settings.

Thus, the proposed multimodal prediction model for neurological disorders using bioinspired transfer learning has shown promising results and has potential for various real-world applications. Further research in the areas mentioned above can enhance the model's performance and utility in clinical settings.

Acknowledgement:

I would like to express my sincere gratitude to all those who contributed to this work. I also appreciate the assistance provided by G.H. Raisoni College of Engineering and Management for their resources and expertise. Finally, my heartfelt thanks to my colleagues and friends for their encouragement and constructive feed back

Author contributions

J.L. Mudegaonkar[1]: Conceptualization, Methodology, Field study, Data curation, Writing-Original draft preparation, Software, Validation., Field study.

D. M. Yadav[2]: Visualization, Investigation, Writing-Reviewing and Editing.

Conflicts of interest

The authors declare no conflicts of interest.

References

[1] M. Qiao et al., "Breast Tumor Classification Based on MRI-US Images by Disentangling Modality Features," in IEEE Journal of Biomedical and Health Informatics, vol. 26, no. 7, pp. 3059-3067, July 2022, doi: 10.1109/JBHI.2022.3140236.

[2] S. Montaha, S. Azam, A. K. M. R. H. Rafid, M. Z. Hasan, A. Karim and A. Islam, "TimeDistributed-CNN-LSTM: A Hybrid Approach Combining CNN and LSTM to Classify Brain Tumor on 3D MRI Scans Performing Ablation Study," in IEEE Access, vol. 10, pp. 60039-60059, 2022, doi: 10.1109/ACCESS.2022.3179577.

[3] J. -W. Zhang et al., "DINs: Deep Interactive Networks for Neurofibroma Segmentation in Neurofibromatosis Type 1 on Whole-Body MRI," in IEEE Journal of Biomedical and Health Informatics, vol. 26, no. 2, pp. 786-797, Feb. 2022, doi: 10.1109/JBHI.2021.3087735.

[4] E. Kim, H. -H. Cho, J. Kwon, Y. -T. Oh, E. S. Ko and H. Park, "Tumor-Attentive Segmentation-Guided GAN for Synthesizing Breast Contrast-Enhanced MRI Without Contrast Agents," in IEEE Journal of Translational Engineering in Health and Medicine, vol. 11, pp. 32-43, 2023, doi: 10.1109/JTEHM.2022.3221918.

[5] M. Ismail et al., "Radiomic Deformation and Textural Heterogeneity (R-DepTH) Descriptor to Characterize Tumor Field Effect: Application to Survival Prediction in Glioblastoma," in IEEE Transactions on Medical

Imaging, vol. 41, no. 7, pp. 1764-1777, July 2022, doi: 10.1109/TMI.2022.3148780

[6] K. Venkatachalam, S. Siuly, N. Bacanin, S. Hubálovský and P. Trojovský, "An Efficient Gabor Walsh-Hadamard Transform Based Approach for Retrieving Brain Tumor Images From MRI," in IEEE Access, vol. 9, pp. 119078-119089, 2021, doi: 10.1109/ACCESS.2021.3107371.

[7] G. J. Ferdous, K. A. Sathi, M. A. Hossain, M. M. Hoque, and M. A. A. Dewan, "LCDEiT: A Linear Complexity Data-Efficient Image Transformer for MRI Brain Tumor Classification," in IEEE Access, vol. 11, pp. 20337-20350, 2023, doi: 10.1109/ACCESS.2023.3244228.

[8] R. Cristin, K. S. Kumar, and P. Anbhazhagan, "Severity Level Classification of Brain Tumor based on MRI Images using Fractional-Chicken Swarm Optimization Algorithm," in The Computer Journal, vol. 64, no. 10, pp. 1514-1530, June 2021, doi: 10.1093/comjnl/bxab057.

[9] Y. Zhang et al., "DeepRecS: From RECIST Diameters to Precise Liver Tumor Segmentation," in IEEE Journal of Biomedical and Health Informatics, vol. 26, no. 2, pp. 614-625, Feb. 2022, doi 10.1109/JBHI.2021.3091900.

[10] N. S. Syazwany, J. -H. Nam and S. -C. Lee, "MM-BiFPN: Multi-Modality Fusion Network With Bi-FPN for MRI Brain Tumor Segmentation," in IEEE Access, vol. 9, pp. 160708-160720, 2021, doi: 10.1109/ACCESS.2021.3132050.

[11] Y. Liu, F. Mu, Y. Shi, and X. Chen, "SF-Net: A Multi-Task Model for Brain Tumor Segmentation in Multimodal MRI via Image Fusion," in IEEE Signal Processing Letters, vol. 29, pp. 1799-1803, 2022, doi: 10.1109/LSP.2022.3198594.

[12] M. A. Ottom, H. A. Rahman and I. D. Dinov, "Znet: Deep Learning Approach for 2D MRI Brain Tumor Segmentation," in IEEE Journal of Translational Engineering in Health and Medicine, vol. 10, pp. 1-8, 2022, Art no. 1800508, doi: 10.1109/JTEHM.2022.3176737.

[13] C. Chen et al., "Synthesizing MR Image Contrast Enhancement Using 3D High-Resolution ConvNets," in IEEE Transactions on Biomedical Engineering, vol. 70, no. 2, pp. 401-412, Feb. 2023, doi: 10.1109/TBME.2022.3192309.

[14] E. A. A. Alaoui, S. C. K. Tekouabou, S. Hartini, Z. Rustam, H. Silkan and S. Agoujil, "Improvement in automated diagnosis of soft tissues tumors using machine learning," in Big Data Mining and Analytics, vol. 4, no. 1, pp. 33-46, March 2021, doi: 10.26599/BDMA.2020.9020023.

[15] T. Zhou, S. Canu, P. Vera and S. Ruan, "Latent Correlation Representation Learning for Brain Tumor Segmentation With Missing MRI Modalities," in IEEE Transactions on Image Processing, vol. 30, pp. 4263-4274, 2021, doi: 10.1109/TIP.2021.3070752.

[16] K. Scheufele, S. Subramanian and G. Biros, "Fully Automatic Calibration of Tumor-Growth Models Using a Single mpMRI Scan," in IEEE Transactions on Medical Imaging, vol. 40, no. 1, pp. 193-204, Jan. 2021, doi: 10.1109/TMI.2020.3024264.

[17] C. Yan, J. Ding, H. Zhang, K. Tong, B. Hua, and S. Shi, "SEResU-Net for Multimodal Brain Tumor Segmentation," in IEEE Access, vol. 10, pp. 117033-117044, 2022, doi: 10.1109/ACCESS.2022.3214309.

[18] H. Cindrič et al., "Retrospective Study for Validation and Improvement of Numerical Treatment Planning of Irreversible Electroporation Ablation for Treatment of Liver Tumors," in IEEE Transactions on Biomedical Engineering, vol. 68, no. 12, pp. 3513-3524, Dec. 2021, doi: 10.1109/TBME.2021.3075772.

[19] A. Kujur, Z. Raza, A. A. Khan, and C. Wechtaisong, "Data Complexity Based Evaluation of the Model Dependence of Brain MRI Images for Classification of Brain Tumor and Alzheimer's Disease," in IEEE Access, vol. 10, pp. 112117-112133, 2022, doi: 10.1109/ACCESS.2022.3216393.

[20] S. Asif, W. Yi, Q. U. Ain, J. Hou, T. Yi, and J. Si, "Improving Effectiveness of Different Deep Transfer Learning-Based Models for Detecting Brain Tumors From MR Images," in IEEE Access, vol. 10, pp. 34716-34730, 2022, doi: 10.1109/ACCESS.2022.3153306.

[21] T. A. Soomro et al., "Image Segmentation for MR Brain Tumor Detection Using Machine Learning: A Review," in IEEE Reviews in Biomedical Engineering, vol. 16, pp. 70-90, 2023, doi: 10.1109/RBME.2022.3185292.

[22] A. U. Haq et al., "IIMFCBM: Intelligent Integrated Model for Feature Extraction and Classification of Brain Tumors Using MRI Clinical Imaging Data in IoT-Healthcare," in IEEE Journal of Biomedical and Health Informatics, vol. 26, no. 10, pp. 5004-5012, Oct. 2022, doi: 10.1109/JBHI.2022.3171663.

[23] A. Anaya-Isaza, L. Mera-Jiménez, and A. Fernandez-Quilez, "CrossTransUnet: A New Computationally Inexpensive Tumor Segmentation Model for Brain MRI," in IEEE Access, vol. 11, pp. 27066-27085, 2023, doi: 10.1109/ACCESS.2023.3257767.

[24] J. Jiang, A. Rimner, J. O. Deasy and H. Veeraraghavan, "Unpaired Cross-Modality Educed Distillation

(CMEDL) for Medical Image Segmentation," in IEEE Transactions on Medical Imaging, vol. 41, no. 5, pp. 1057-1068, May 2022, doi: 10.1109/TMI.2021.3132291.

[25] R. Zheng et al., "Automatic Liver Tumor Segmentation on Dynamic Contrast Enhanced MRI Using 4D Information: Deep Learning Model Based on 3D Convolution and Convolutional LSTM," in IEEE Transactions on Medical Imaging, vol. 41, no. 10, pp. 2965-2976, Oct. 2022, doi 10.1109/TMI.2022.3175461.

[26] H. A. Shah, F. Saeed, S. Yun, J. -H. Park, A. Paul and J. -M. Kang, "A Robust Approach for Brain Tumor Detection in Magnetic Resonance Images Using Finetuned EfficientNet," in IEEE Access, vol. 10, pp. 65426-65438, 2022, doi: 10.1109/ACCESS.2022.3184113.

[27] S. Subramanian, A. Ghafouri, K. M. Scheufele, N. Himthani, C. Davatzikos and G. Biros, "Ensemble Inversion for Brain Tumor Growth Models With Mass Effect," in IEEE Transactions on Medical Imaging, vol. 42, no. 4, pp. 982-995, April 2023, doi: 10.1109/TMI.2022.3221913.

[28] F. Fang, Y. Yao, T. Zhou, G. Xie, and J. Lu, "Self-Supervised Multi-Modal Hybrid Fusion Network for Brain Tumor Segmentation," in IEEE Journal of Biomedical and Health Informatics, vol. 26, no. 11, pp. 5310-5320, Nov. 2022, doi: 10.1109/JBHI.2021.3109301.

[29] K. Ejaz, M. S. M. Rahim, U. I. Bajwa, H. Chaudhry, A. Rehman, and F. Ejaz, "Hybrid Segmentation Method With Confidence Region Detection for Tumor Identification," in IEEE Access, vol. 9, pp. 35256-35278, 2021, doi: 10.1109/ACCESS.2020.3016627.

[30] M. Rahimpour et al., "Cross-Modal Distillation to Improve MRI-Based Brain Tumor Segmentation With Missing MRI Sequences," in IEEE Transactions on Biomedical Engineering, vol. 69, no. 7, pp. 2153-2164, July 2022, doi: 10.1109/TBME.2021.3137561.